Long-range acoustic localization of artillery shots using distributed synchronous acoustic sensors

Adrien Dagallier,[1,a)] Sylvain Cheinet,[1] Matthias Cosnefroy,[1,b)] Winfried Rickert,[2] Thomas Weßling,[2] Pierre Wey,[1] and Daniel Juvé[3]

[1]*French-German Research Institute of Saint-Louis, 5 rue du Général Cassagnou, 68300 Saint-Louis, France*
[2]*Wehrtechnische Dienststelle 91, Schiessplatz, D49716 Meppen, Germany*
[3]*Université de Lyon, Ecole Centrale de Lyon, Laboratoire de Mécanique des Fluides et d'Acoustique, Unité Mixte de Recherche, Centre National de la Recherche Scientifique 5509, Ecully, F-69134, France*

(Received 1 February 2019; revised 24 July 2019; accepted 24 July 2019; published online 31 December 2019)

Acoustic recordings of artillery shots feature the signatures of the shot's muzzle, projectile, and impact waves modulated by the environment. This study aims at improving the sensing of such shots using a set of synchronous acoustic sensors distributed over a 1 km^2 area. It uses the time matching approach, which is based on finding the best match between the observed and pre-calculated times of arrivals of the various waves at each sensor. The pre-calculations introduced here account for the complex acoustic source with a 6-degrees-of-freedom ballistic trajectory model, and for the propagation channel with a wavefront-tracking acoustic model including meteorological and terrain effects. The approach is demonstrated using three recordings of artillery shots measured by sensors which are more than 10 km from the point of fire and distributed at several hundred meters away from and around the target points. Using only the impact wave, it locates the impact point with an error of a few meters. Processing the muzzle and impact and projectile waves enables the estimation of the weapon's position with a 1 km error. Sensitivities of the localization method to various factors such as the number of sensors, atmospheric data, and the number of processed waves are discussed.
 https://doi.org/10.1121/1.5138927

[KTW] Pages: 4860–4872

I. INTRODUCTION

Localization of artillery shots brutally became of concern in 1914.[1] Being passive, all-weather, discrete, and non-line-of-sight, acoustic sensing was investigated with great hopes—and at first poor successes. The shells had only recently become supersonic, and even trained listeners could not differentiate the snaps belonging to the muzzle blast from those coming from the ballistic shock wave emitted along the trajectory by the supersonic projectile, which resulted in haphazard localizations. The discovery of infrasounds in artillery by Esclangon[2] led to the invention of manometers specifically designed for the characteristic slow oscillations of the muzzle blast. Times of Arrival (TOAs) could be reliably ascribed to the muzzle blast and the shock wave of the supersonic projectile was discarded. The localization itself was entrusted to a team of expert computers that could locate the sound source from the muzzle wave TOAs within a few minutes.

Since then, detection and classification procedures have been improved and largely automatized,[3] sensors are much more sensitive, and wireless communications allow fast system deployments over broad areas.[4] Determination of bearings from TOAs by synchronous pairs of sensors[1] turned into cross-bearings determined from multiple asynchronous arrays of synchronous sensors.[4,5] Yet the localization itself has not changed much and is still based on the muzzle blast. The ballistic shock wave is often not even mentioned in recent articles.

Achieving a bearing from an array is relatively straightforward for loud impulse sounds, whatever the distance between the array and the sound source. For ranging, though, this geometry remains a stringent constraint.[6–9] Following, e.g., Thompson and Durfee,[6] the ratio $r = l/L$ is introduced, where l is the characteristic size of the sensors array and L the source-array distance. Achieving accurate ranging is usually thought to require a large baseline array, i.e., with $r \sim 1$.[4–7] Conversely, ranging artillery sounds in the case $r \ll 1$ (small baseline array) has never been demonstrated.

Depending on the range, the atmosphere, the ground, possible obstacles (woods, buildings, hills…), refraction[10] or air absorption,[11] the various waves emitted by and during a shot may undergo such alterations as to become hardly recognizable. The type and amount of explosive charge in the shell dramatically alter the impact acoustic signature and possibly the directionality of the explosion. The ballistic shock wave and later multipath arrivals, emitted along the trajectory because of the initial supersonic velocity, may be seen as a large amplitude, broadband signal that lasts for more than one second and tends to drown out all the signals recorded in that interval. The recorded number of arrivals and their order depend on the shot configuration, the

a)Also at: Université de Lyon, Ecole Centrale de Lyon, Laboratoire de Mécanique des Fluides et d'Acoustique, Unité Mixte de Recherche, Centre National de la Recherche Scientifique 5509, Ecully, F-69134, France. Electronic mail: adrien.dagallier@isl.eu

b)Also at: Université de Lyon, Ecole Centrale de Lyon, Laboratoire de Mécanique des Fluides et d'Acoustique, Unité Mixte de Recherche, Centre National de la Recherche Scientifique 5509, Ecully, F-69134, France.

obstacles, and the atmospheric wind and sound speed gradients. The projectile trajectory itself is affected by the environment since most aerodynamic coefficients depend on the Mach number, which is a function of the local sound speed and wind. Localization performance is affected, sometimes critically.[12]

In recent years, the matching method for localization of point sources in complex, known environments has been developed.[13] This method consists of pre-computing a database of acoustic features at each microphone for all possible source positions. The pre-calculation factors in the full complexity of the propagation channel. The source position is estimated by determining, from the database, the source position for which the predicted acoustic features at each microphone best match the measurements. Among all the acoustic features of operational interest (frequency spectra, temporal signals, directions of arrival, or times of arrival[13,14]), TOAs are the most robust ones. This makes it practical to work on TOAs, and the method can then be referred to as time matching. Note that the actual quantities of interest are the differences in TOAs (DTOAs). Following Cheinet *et al.*,[13,14] the denomination TOA is, however, kept to avoid confusion with so-called DTOA methods, which refer to estimating a direction of arrival from pairs of sensors, or to computing the time delay between the arrival of the muzzle blast and ballistic shock wave at each sensor or between the arrival of the ballistic shock wave at each pair of sensors.[1,3–9,15]

This paper extends the matching approach to isolated artillery shots by building a numerical database of TOAs of the impact signal, ballistic shock wave, and muzzle blast through coupled ballistic–acoustic simulations. The ballistic model parameters and the atmospheric data are assumed to be known. It investigates whether the resulting processing, accounting for the complex artillery sound source and propagation effects in a consistent way, is able to locate the impact point and the weapon. The paper is organised as follows. Section II introduces the matching approach and the acoustic model. Section III applies the approach to point source localization for sources within the sensor array using the impact wave only (impact point localization) or far away from the array using the muzzle blast only (gun localization). Section IV includes the ballistic shock wave and the ballistics of the projectile in the processing. Section V discusses the sensitivities of the approach to various factors such as atmospheric data, the number of sensors, and the number of processed waves. Section VI provides a conclusion.

II. MATCHING AND MARCHING APPROACH

A. Matching localization of point sources

The principle of the time matching approach for point source localization[13,14] is here briefly recalled. The domain of interest is first discretized in a three-dimensional (3D) mesh. Each element of the mesh, of index j, can be thought of as a possible source location. For each source location, a numerical simulation of an impulse sound propagation is performed, from which the TOA is calculated at each sensor (index i_{mic}, $i_{mic} = 1 \ldots N$, with N the number of sensors). The overall procedure produces the TOA database $(t_{i_{mic}j})$. In practice, the simulations may be run from each sensor to all mesh points, which reduces the number of simulations down to N and thus the computation time.

Upon detection of an event, the TOA $\hat{t}_{i_{mic}}$ is obtained (the hat standing for observations). Let i_0, $1 \leqslant i_0 \leqslant N$, denote the index of a reference microphone, taken as, e.g., the sensor of first signal arrival. Let $\Delta t_{i_{mic},j} = t_{i_{mic},j} - t_{i_0,j}$ denote the predicted differential TOA of the signal at microphones i_{mic} and i_0, emitted by the source at location j, and define $\hat{\Delta}_{i_{mic}} = \hat{t}_{i_{mic}} - \hat{t}_{i_0}$. When the source location j is the actual source position, $\Delta t_{i_{mic},j} \simeq \hat{\Delta} t_{i_{mic}}$ for all i_{mic}. Let us define the cost function[13,14]

$$E_j = \sum_{\substack{i_{mic}=1 \\ i_{mic} \neq i_0}}^{N} (\hat{\Delta} t_{i_{mic}} - \Delta t_{i_{mic},j})^2. \tag{1}$$

Let us define the localization index $C_j = 1/\sqrt{E_j/(N-1)}$. C_j is highest where the predicted TOAs match the measured ones in a least-square sense. It is our basic localization metrics. The simplest way of calculating the TOAs is an analytical model *time = distance/sound speed*, assuming line-of-sight and homogeneous atmosphere. In this case, the time matching approach reduces to a simple multi-lateration method based on TOAs. One key aspect of the matching approach is that the propagation modeling in the preparatory step may account for the effects of the propagation channel on the TOAs. For urban environments, Cheinet *et al.*[13,14] use a 3D solver based on the finite-difference time-domain method (FDTD). Such a solver is very general and can handle non-line-of-sight propagation and inhomogeneous atmospheres. However, the full time-dependent pressure field is computed with the FDTD, which is both computationally demanding and unnecessary in the context of Eq. (1)—only the signal TOA is useful. In the remainder of this section, another TOA calculation approach is introduced, namely, a 3D interface-tracking solver. It applies to the same propagation media as the FDTD but restricts to TOA calculations and is thus much faster.

B. Interface tracking

Let us consider a sound wave propagating in an arbitrary medium. In a frame moving with the medium, the apparent wavefront velocity at point $\boldsymbol{x}$ and time t is $c(\boldsymbol{x},t)\boldsymbol{n}(\boldsymbol{x},t)$, where $\boldsymbol{n}$ is the normal to the wavefront and

$$c(\boldsymbol{x},t) = \sqrt{\gamma R T(\boldsymbol{x},t)(1+\alpha h(\boldsymbol{x},t))}$$

is the time-dependent local sound speed, where $\gamma = 1.4$ is the specific heat ratio, $R = 287.05$ J/kg/K the specific gas constant, T and h the local temperature and specific humidity[16] (in kg·kg^{-1}), and $\alpha = 0.511$. In a frame at rest, it becomes

$$\boldsymbol{c_{eff}}(\boldsymbol{x},t) = c(\boldsymbol{x},t)\boldsymbol{n}(\boldsymbol{x},t) + \boldsymbol{v}(\boldsymbol{x},t), \tag{2}$$

where $\boldsymbol{v}$ is the local velocity of the fluid. Let P be a point on the wavefront $t = F(\boldsymbol{x})$ and let $\boldsymbol{x}_P(t)$ be its position at time t. P remains on the wavefront if

$$\frac{d\boldsymbol{x}_P}{dt} = \boldsymbol{c}_{eff}(\boldsymbol{x}_P, t). \quad (3)$$

This equation completely describes the wavefront completely, but the presence of $\boldsymbol{n}$ makes it difficult to use for proper computations. The position of P at time $t + dt$ is $\boldsymbol{x}_P(t+dt) \approx \boldsymbol{x}_P(t) + \dot{\boldsymbol{x}}_P(t)dt$, and one has $t + dt \approx F(\boldsymbol{x}_P) + \dot{\boldsymbol{x}}_P dt \cdot \nabla F$. Since $t = F(\boldsymbol{x}_P)$, one has $\dot{\boldsymbol{x}}_P \cdot \nabla F = 1$. Besides, $\nabla F(\boldsymbol{x}_P)$ is normal to the surface $t = F(\boldsymbol{x})$ and therefore collinear with $\boldsymbol{n}$. With $\nabla F = ||\nabla F||\boldsymbol{n}$, Eq. (3) becomes

$$||\nabla F||(c + \boldsymbol{n} \cdot \boldsymbol{v}) = 1. \quad (4)$$

Equation (4) may lead to the ray equations and subsequent TOA calculations when integrated along a ray (see, e.g., Ref. 17, Sec. 8.1). Alternatively, wavefront approaches use Eq. (4) to propagate the wavefront through the medium, so that TOAs are obtained at every point of the meshed domain. These wavefront methods come in several flavors, based on the Huygens principle. Shortest path methods draw upon graph theory,[18–20] while finite-difference approaches compute the continuous wavefront surface.[21,22] Among the latter, Sethian *et al.*[23] have developed an Eulerian solver, called the Fast-Marching method.

C. Acoustic model

In this study, the used solver of Eq. (4) is based on the model of Sethian and Vladimirsky.[24] This choice is motivated by the generality of their formulation. It addresses general anisotropic problems, where the wavefront propagation depends not only on the position of the front, but also on the direction of propagation,[23,24] e.g., due to wind in atmospheric acoustics, or to currents in underwater acoustics. This approach readily applies to seismic acoustics,[25,26] underwater acoustics,[27] and other applications such as signal denoising or path-planning. The model of Sethian and Vladimirsky is developed for two-dimensional (2D) unstructured meshes. Our implementation extends it to 3D media and uses a Cartesian grid. Anisotropy is accounted for by a retroaction loop[28] and the implementation of Yatziv *et al.*[29] is retained for its efficiency. The present implementation is hereafter referred to as the IFM (Institute Saint-Louis Fast-Marching Model). The IFM propagates the interface of a "known" subdomain in an "unknown" domain (Fig. 1). The algorithm starts from an initial "known" subdomain, e.g., a single point for an acoustic point source. The interface between the "known" and the "unknown" parts, which is the set of points at the boundary of the "known" domain, is then updated as follows: find the point with the smallest TOA in the interface, move it to the "known" domain, compute its neighbors' TOAs and add them to the interface. The TOAs are computed from the "known" points by means of Eq. (4). The algorithm stops when all points are "known." For validation purposes, a comparison between the interface propagation of the IFM and a FDTD solver for the linearized Euler equations[30] is shown in Fig. 2 for a wave emitted by a point source in a medium with strong sound speed contrasts (300–400 m/s) and some reflective and diffractive obstacles. The resulting pressure field is displayed for five different snapshots. Superposed is the wavefront as computed with the IFM. The match is very good, including both in areas with (de)focusing and behind obstacles, where only diffracted waves can propagate and classical ray approach is not applicable. The computation time is on the order of 5 min on a 4 CPUs computer for the time domain simulation, against about one second on 1 CPU for the IFM on the same grid. As Fig. 2 highlights, however, the speedup is at the expense of all information regarding the pressure time series. The IFM predicts exclusively the TOA of the first wavefront to arrive. More extensive discussions on the numerical errors of the Fast-Marching method may be found in the literature.[25] The errors are well-below the uncertainty levels of the TOA estimation in the experimental data. Note that ground reflections do not need to be modeled, since they necessarily arrive after the first TOAs computed by the IFM. In summary, the localization steps are (i) the preparatory TOA determination with IFM in the known, complex environment, then (ii) a minimization of Eq. (1) using the observed TOAs. The method is hereafter referred to as matching-and-marching approach, as it combines the time matching principle with the fast-marching propagation model.

III. APPLICATION TO POINT SOURCE LOCALIZATION

The point source localization approach outlined in Sec. II A is now tested for the impact's wave and the weapon's muzzle blast taken separately. The analysis is based on an experimental dataset of three artillery shots. For each shot, the weapon, impact and microphone positions, as well as

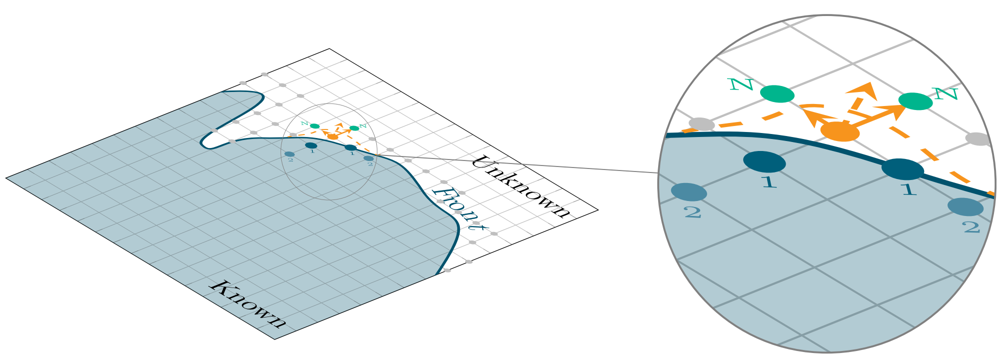

FIG. 1. (Color online) Algorithm's principle. The "known" TOA domain is the filled area, the small gray disks and the dark line represent the current interface. The point with the smallest TOA is picked from the interface. The local direction of propagation is given by the gradient to the interface (arrows), with finite difference schemes of first ("1") or second ("2") order. The neighbor points ("*N*") are added to the interface (dashed line) with their estimated TOA.

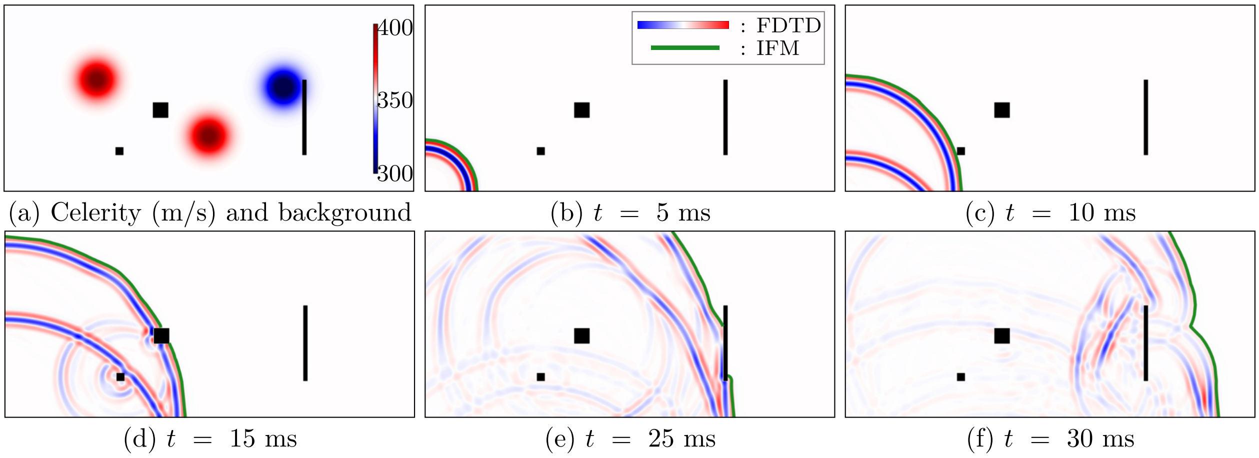

FIG. 2. (Color online) Comparison FDTD-IFM. (a) Simulation domain with strong sound speed variations and obstacles. (b)–(f) snapshots of the FDTD and IFM simulations. The colormap is used for the FDTD pressure field. The thick line is the wavefront computed by the IFM.

the projectile's muzzle velocity and the elevation and azimuth angles of the barrel were observed. The shots took place between 15 and 16 h on June 7, 2011, at Meppen Proving Ground, North West Germany. Synchronous acoustic data from $N = 6$ microphones were recorded. They are located about 13 km away from the weapon, and at distances between 100 and 1000 m from the impact points. For such distances, the assumption of point source emission is deemed to be valid for the muzzle blast. It should also be applicable to the impact explosion if the sounds emitted by supersonic fragments of the shell or of the ground are negligible compared to or indistinguishable from the explosion blast itself.

The acoustic recordings are shown on Figs. 3(a)–3(c). For each of the three shots, the first wave arriving at each sensor is the ballistic shock wave, which has a rise time of a few samples, followed by a high frequency content tail. Then comes either the impact wave (shot 1 and 2) or the muzzle blast (shot 3), depending on the shot configuration. The muzzle blast is a low frequency wave, its high frequency content being lost due to atmospheric absorption. For each recorded shot, the muzzle blast is followed by a second arrival [Fig. 3(d)]. It is presumed that the latter is due to the refraction by inversions in atmospheric temperature and wind along the shot axis [see also Fig. 7(a) below, at a height of around 2 km]. The impact signal is generated as the projectile hits the ground close to the sensor array. As illustrated by Fig. 3(d), the signature of the impact explosion varies more markedly from microphone to microphone than the ballistic shock wave and muzzle blast arrivals. Besides a possible anisotropy of the explosion, the near-field pressure signal may undergo various propagation conditions from the impact point to the various sensors:[10] favorable vs unfavorable wind, close range vs far away from the sensor.

The sampling frequency of the microphones used in this study is 1 kHz, which is deemed sufficient for artillery guns sound signals. The arrivals are classified from visual inspection (Fig. 3), and the TOAs are determined as the times at which the acoustic pressure first reaches $p_{max}/10$, where p_{max} is the first pressure peak in the considered arrival. Here, the actual TOA measurement error is always smaller than the rise time of the signal, which ranges between 1 ms (ballistic shock waves) and 50 ms (muzzle blast, shot 3).

A. Localization of the impact point

The matching-and-marching approach is now applied to test localization of the impact explosion based on the impact TOAs only. The observed impact points are within or close to the sensors array, so that for these sound sources, the array is with $r \sim 1$ (Sec. I). For the TOA precalculations, the IFM domain is of size 1.6 km $\times$ 1.6 km $\times$ 0.2 km, and the model is run with a Cartesian grid of step 5 m in all directions. The temperature profile is derived from the standard atmosphere model[31] (see Fig. 7), with a ground temperature of 16 °C, without wind. The TOA database calculation takes less than 5 min on a single CPU. The domain is meshed in 3D, but hereafter only ground level localization maps are shown.

The localization results are gathered in Table I. The errors are on the order of 5 m. This uncertainty is on the order of the model grid spacing. It is also on the order of the spatial uncertainty resulting from the TOA estimation inaccuracies. Furthermore, the explosion itself generates a shock wave in the near field, whose supersonic propagation over the first ~10 m is not accounted for in our (linear) sound propagation model (extension of the Fast-Marching scheme to non-linear shock wave physics should, however, be possible[32]). The map of the localization index C_j is shown in Fig. 4(a) for shot 2. The small spread of the high localization index region[13,14] suggests that the localization is reliable. Overall, the method compares satisfactorily with the claimed error of commercial systems[4,15,33] and of acoustic systems used on artillery proving grounds for impact localization.

Taking the reported near-surface wind (3 m/s near the surface, in the direction of the shot) into account neither improves nor deters the above impact localizations. This wind magnitude is on the order of 1% of the sound speed, and will thus affect the localization on the order of 1%, or 1–10 m in the considered shots (Table I). Such a correction is not significant enough to be seen given the aforementioned 5 m discretization. In the general case, the effect of wind speed on localization could be non-linear. In the present

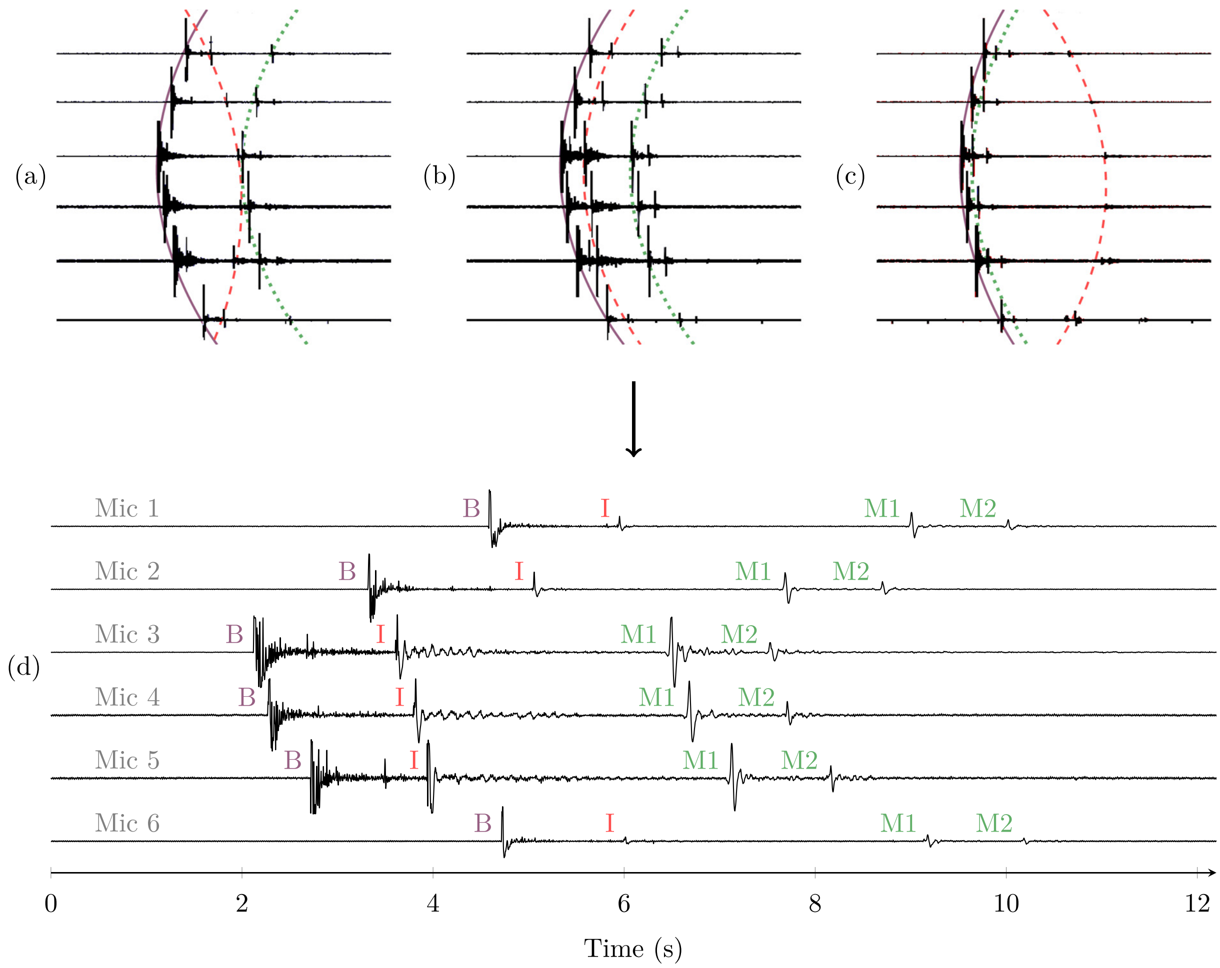

FIG. 3. (Color online) (a)–(c) Acoustic recordings at the six microphones (sampling frequency 1 kHz) of the three shots. The solid (resp. dashed, dotted) curves on the recordings indicate the arrivals of the ballistic (resp. impact, muzzle) waves. They are a guide to the eye. (d) Zoom on shot 2. The arrivals of the ballistic (resp. impact, muzzle) waves are tagged with the letter "B" (resp. "I", "M"). Two muzzle blast arrivals are visible.

scenario, all conducted tests suggest that such a non-linearity does not affect the results significantly.

B. Localization of far-away point sources

The matching-and-marching approach is now applied to locate the weapon based solely on the muzzle blast TOAs. In that case, the sound source is at a large distance from the sensors, so that one has $r \ll 1$. For the TOA precalculations in that case, the IFM domain is of size 54×8 km in the X and Y directions, respectively, for a height of 4 km, and the IFM model is run with a Cartesian grid of step $100 \times 100 \times 20$ m. The standard atmosphere model is used[31] without wind. Computing the TOAs in the whole domain takes less than 10 min on a single CPU.

TABLE I. Impact localization error, defined as the distance between the measured and computed impact points.

	Localization error (m)	
Point	No wind	Wind
Impact 1	6.3	2.2
Impact 2	9.5	3.2
Impact 3	3.6	13.2

In that case, the localization approach estimates the bearing of the sound source [Fig. 4(b)]. The bearing is slightly off, which is presumably due to the neglect of wind in computing the TOAs. Besides, the range estimate shows

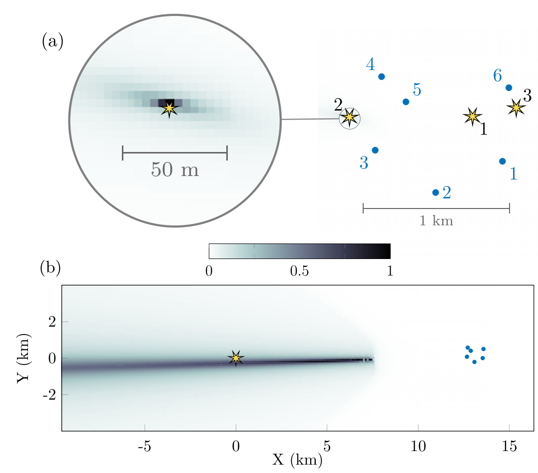

FIG. 4. (Color online) (a) Localization of the impact. Distributed sensors (dots), numbered from 1 to 6, and impacts positions (stars), from 1 to 3. The normalized localization index (C_j) for the impact of shot 2 is displayed in inset. The darker the color, the higher the localization index. (b) Normalized localization index for the weapon localization, shot 2.

errors on the order of the range. Such large errors are typical of ranging from small baseline arrays. Operational sensing systems based on small baseline arrays usually estimate the source bearing without ranging.[5,6] The reported error of 2°–3° in Fig. 4 is in line with the literature[5–7,12] and may be related to the low characteristic frequencies and background noise contamination of the muzzle blast after 13 km of propagation (inaccurate TOA estimation), as well as to random TOA fluctuations at the sensors due to atmospheric turbulence along the path, and to possible terrain variations (woods, buildings, etc.).

In the above localization tests, the weapon is localized based on the muzzle blast TOAs, while the impact position is estimated from the impact TOAs. In other words, the physical, consistent link between these acoustic data is ignored. The ballistic wave is ignored as well, which is questionable on a sensing point of view: the ballistic shock wave has the largest amplitude, a sharp rise and a characteristic tail (Fig. 3). It is thus straightforward to detect and classify. Furthermore, this wave is emitted in the bulk atmosphere, and its TOA is therefore less sensitive to ground obstacles (buildings), topography (hills, mountains), or near-surface atmospheric gradients than the muzzle and impact sounds. Later multipath arrivals do not affect the TOA estimation. In Sec. IV, the matching-and-marching approach is adapted to consistently process all three types of sounds emitted by an artillery shot.

IV. ARTILLERY SHOT LOCALIZATION

A. Principle

The TOA matching method can be extended to utilize all three types of sounds emitted by an artillery shot. The shot parameters to be estimated are the weapon position, the muzzle velocity, and the barrel elevation and azimuth. For a given pre-determined discretization of these parameters, let us introduce their respective indices j, v, e, a. Let us denote by $t^{ballistic}_{i_{mic},v,e,a,j}$ the TOA at sensor i_{mic} due to projectile sound for the shot configuration specified by the shot indices j, v, e, a. Likewise, let us define $t^{muzzle}_{i_{mic},v,e,a,j}$ and $t^{impact}_{i_{mic},v,e,a,j}$ for the TOAs due to the muzzle blast and impact explosion of this shot, respectively. The matching localization consists of finding the set of shot parameters that minimizes the sum of differences between the observed and predicted relative TOAs for all three types of sounds over all sensors, i.e., by minimizing the following cost function:

$$S_{j,v,e,a} = \sum_{\substack{i_{mic}=1 \\ i_{mic}\neq i_0}}^{N} \left(\hat{\Delta}t^{ballistic}_{i_{mic}} - \Delta t^{ballistic}_{i_{mic},v,e,a,j}\right)^2 + \sum_{i_{mic}=1}^{N} \left(\hat{\Delta}t^{muzzle}_{i_{mic}} - \Delta t^{muzzle}_{i_{mic},v,e,a,j}\right)^2 + \sum_{i_{mic}=1}^{N} \left(\hat{\Delta}t^{impact}_{i_{mic}} - \Delta t^{impact}_{i_{mic},v,e,a,j}\right)^2, \quad (5)$$

where the Δt s for each type of sound are relative TOAs defined in a similar way to Eq. (1), with the reference TOA being the TOA of the ballistic shock wave arrival at sensor i_0 (corresponding to the first arrival on the array). The set of parameters $(j', v', e', a') = \text{argmin}_{j,v,e,a}\{S_{j,v,e,a}\}$ minimizing this cost function provides the best estimates of the position of the gun, the muzzle velocity, and the barrel elevation and azimuth angles. The localization index is now defined as $C_j = 1/\sqrt{E_j/(3N-1)}$, where N is the number of sensors and $E_j = \min_{v,e,a}\{S_{j,v,e,a}\}$. The precalculation of the TOAs in Eq. (5) is now addressed. For use in actual localization, these TOAs have to be modeled with a sufficient degree of physical realism and consistency. The muzzle and impact waves are seen as point sources and are modeled as in Sec. III. The projectile's wave is modeled by combining a ballistic trajectory model to the IFM, as now detailed.

Artillery projectiles travel large distances, at possibly supersonic speeds and at large incidence angles. To ensure that the multiple aerodynamic phenomena are correctly treated, the BALCO software[34] is used. BALCO is a NATO 6 degrees-of-freedom (position plus angular rotations) standard numerical model (STANREC 4618) to compute high accuracy trajectories in three dimensions. It may be used for a large variety of projectiles and weapons. The model allows for pre- or user-defined gravity, aerodynamic, and atmospheric models. This study restricts to ballistic projectiles, considered as non-propelled, single rigid bodies. Unless otherwise stated, all trajectories are computed with (i) an ellipsoidal Earth gravity model,[35] (ii) projectile and weapon coefficients (lift and drag, Magnus effect, pitch/roll/spin moments, moments of inertia of the projectile, barrel rifling) of a standard French 155 mm ammunition and weapon. The atmospheric model is taken identical to the one used in the sound propagation calculations. Under these assumptions, it is possible to reliably predict the projectile trajectory and its subsequent impact position for any given set of parameters (j, v, e, a).

Acoustically speaking, it is assumed that the ballistic shot sound is emitted only when the projectile is supersonic. Physically, this assumption is motivated by the nonlinear behavior of the ballistic coefficients (drag etc.) around $M = 1$ (e.g., Ref. 36). Here, M is the Mach number, i.e., the ratio of the velocity of the projectile and the local apparent sound speed (accounting for the wind). In practice, the distinction between subsonic and supersonic regimes is probably not so clear-cut. The flow around and along the projectile may be locally supersonic even if $M \leq 1$. Modeling the acoustic behavior of a projectile in this regime is beyond the scope of the present study. From a numerical point of view, the ballistic shock wave TOA $t_{B_{mic}}$ for the supersonic part of a trajectory, $\mathcal{T}$, at a given microphone, is computed as

$$t_{B_{mic}} = \min_{(x,y,z)\in\mathcal{T}} \left\{ t_{\mathcal{T}}(x,y,z) + t_{(x,y,z)\to mic} \right\},$$

where $t_{\mathcal{T}}(x,y,z)$ is the time at which the projectile reaches point (x, y, z) of the BALCO trajectory, and $t_{(x,y,z)\to mic}$ is the acoustic propagation time between the point (x, y, z) and the microphone *mic*. No additional IFM run is required, as the TOAs of all mesh points to the sensors have already been computed.

B. Sound emissions of shot 2

For illustrative purposes, the muzzle, projectile, and impact TOAs are simulated with the combination BALCO-IFM for shot 2 [Fig. 3(d)] with the following parameters: muzzle velocity of 625 m/s, elevation angle of 335 mils, and azimuth angle of -38 mils (NB: 1 mil is approximately $0.056°$), in the standard atmosphere. The various wavefronts are shown on Fig. 5. Locally, the Mach number does not vary much and the projectile's movement is rectilinear, so that the projectile shocks superpose to form a conical Mach wave of aperture angle θ given by $\sin\theta = 1/M$. On snapshot Fig. 5(a), the small conical aperture of the ballistic shock wave reveals that the projectile's velocity is well above the speed of sound.

For artillery shots, the apparent speed of sound [Eq. (2)] significantly varies with height, e.g., due to the temperature decrease. Besides, the projectile's velocity may vary by a factor of 3 along the trajectory, and the projectile may undergo several subsonic-supersonic transitions. The overall emission shape of the projectile is thus more complex than a cone, and is further distorted by the wind and sound speed profiles during its propagation.

From snapshot Fig. 5(b) onwards, the projectile falls slightly behind the ballistic shock wave, as the projectile becomes subsonic. The projectile hits the ground in Fig. 5(c), after 35 s of flight. Its impact position is highlighted on Fig. 4, and generates the impact wave of snapshot [Fig. 5(d)].

C. Shot sensing

The sensing approach introduced in Sec. IV A is now tested on the three shot recordings analyzed above. For these tests, the preparatory database is formed as follows. The source positions are discretized on a horizontal grid of 54 km along the shot axis (X axis), 8 km along the transverse axis (Y axis), with a 200 m spacing in both directions. For each weapon position, the muzzle velocity ranges from 450 to 700 m/s by steps of 10 m/s, the elevation from 250 to 700 mils by steps of 10 mils, and the azimuth angle from -100 to 100 mils by steps of 50 mils. The azimuth discretization is refined (spacing of 5 mils) around the actual shot axis. The present database discretization, though by no means optimal, is devised to ensure that consecutive (x, y, v, e, a) database elements have impacts within 200 m (the grid spacing) from each other. Thus, approximately 8000 shot configurations are scanned for each weapon position. Both BALCO and IFM simulations use the standard atmosphere (no wind). At ground level, one takes $c \approx 341$ m/s.

Figure 6 features the localization indices obtained for the three shots. As will be shown below, the ripples (or multiple peaks) are due to the precalculated database discretization. The 10 km scatter in the weapon's position estimates based solely on the muzzle blast TOAs was analyzed in Sec. III and is here shown for reference. Compared to Sec. III, the weapon position estimates now obtained (with the muzzle blast, ballistic shock wave and impact explosion TOAs) are much closer to the weapon, with an uncertainty on the order of 1 km. The impact point for shot 2 is outside the sensor array, whereas the impacts of shots 1 and 3 are within the array [Fig. 4(a)]. The impact position is therefore less discriminative for shot 2, whereby the localization index tail for $X < 0$ in Fig. 6(d), not seen on Figs. 6(b) and 6(f).

Along with the weapon's position, the proposed method of Sec. IV A also provides estimates of the muzzle velocity, and the elevation and azimuth angles of the barrel (parameters v', e', and a'). For shot 1, the estimated muzzle velocity is of 650 m/s and the elevation is of 330 mils, very close to the actual values (657 m/s and 335 mils, respectively). For shot 2, the corresponding estimates are 620 m/s and 330 mils, compared to the actual values of 625 m/s and 335 mils, respectively. For shot 3, the corresponding estimates are 520 m/s and 500 mils, compared with the actual values of 534 m/s and 540 mils, respectively. Hence, the method provides a reliable indication of the elevation and muzzle velocity of the shot. Other shot parameters of potential interest for operational use may also be obtained as by-products of the calculations, e.g., the time of flight or the propellant charge.

In summary, our results show that the matching and marching approach can be extended to consistently utilize all three types of sounds emitted by an artillery shot. They also suggest that this extension may enable to range the weapon with an error of 1 km at ranges larger than 10 km, despite the small baseline configuration of the sensors array. To our knowledge, this result is unprecedented.

V. DISCUSSION

In this section, the sensitivity of the weapon's localization error to various factors is discussed. From the results of Sec. IV, the typical deviation of the observed TOA from the best predicted TOA scales with $1/C_j \sim 30$–50 ms. The sensitivity analyses should therefore include all effects capable of such alterations of the TOAs: weather effects, random TOA

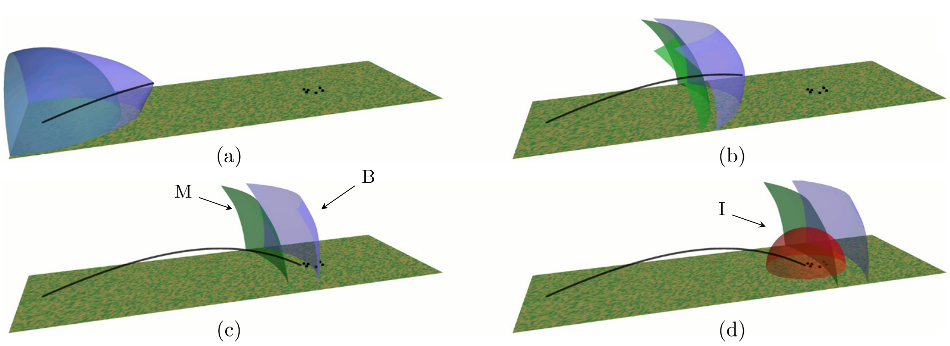

FIG. 5. (Color online) Sketch of shot 2. The muzzle blast, ballistic shock wave and impact signal ("M," "B," and "I," respectively) are displayed at different times. The BALCO trajectory is the black line.

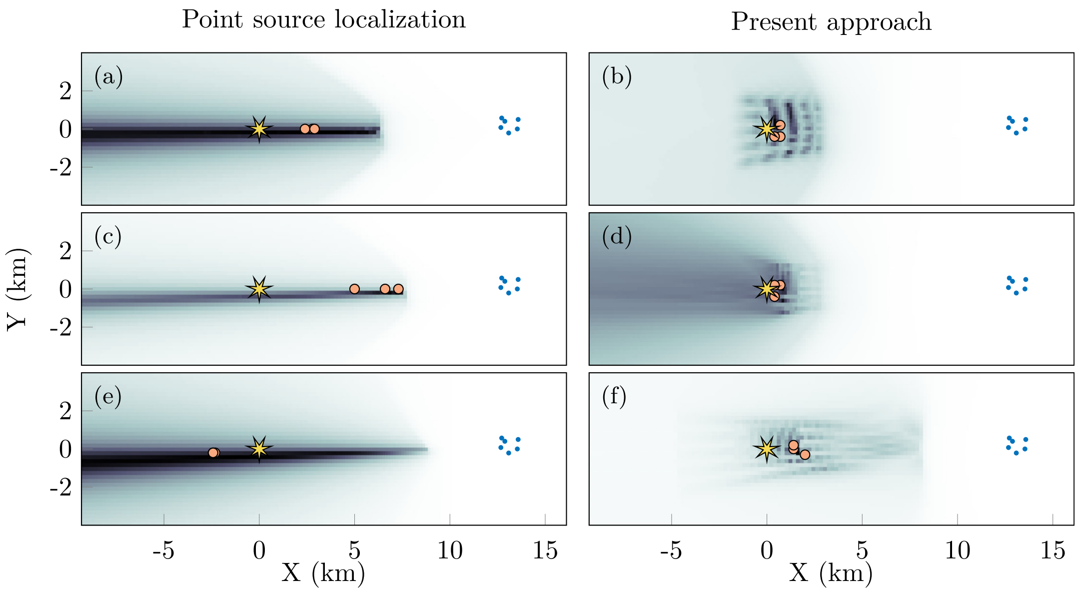

FIG. 6. (Color online) Normalized localization index for long range weapon localization. (a), (c), (e) Point source localization from the muzzle wave TOAs for shots 1, 2, 3, respectively. (b), (d), (f) Localization with processing of the trajectory and muzzle, projectile and impact TOAs for shots 1, 2, 3, respectively. Dots on the right are sensors, the star is the weapon and the circles are the three highest peaks from the map. Same colorbars as in Fig. 4.

fluctuations, and database discretization effects. Other sensitivities considered hereafter are scoped toward practical applications. They include the number of sensors and the geometry of the array, and the performance in the case of degraded information on the TOAs: missing wave, or missing classification.

A. Weather effects

The effect of the wind is acknowledged in line of bearings methods (e.g., Refs. 5 and 7). In our processing, the weather may alter both ballistics and acoustics. On the ballistic side, a wind change of 10 m/s along the shot axis can lead to variations of hundreds of meters in the computed impact's position for 10 km shots with fixed initial parameters. On the acoustic side, the wind can alter the time delay between the ballistic shock wave TOAs (propagation from the projectile towards the ground) and the muzzle blast TOAs (propagation close to the ground, where winds are weaker). For example, a convective wind of 10 m/s alters the muzzle blast's propagation time by almost 1 s over a 30 s propagation, which amounts to a range offset larger than 300 m. Besides, projectiles may reach heights of several kilometers, and the variations in pressure, temperature, Mach number, and through the Mach number, most aerodynamic coefficients are significant.

To test the sensitivity of the above results to the atmospheric conditions, the European Center for Medium Range Weather Forecasts (ECMWF) Re-Analysis (ERA)-Interim weather dataset[37] can be used. ERA-Interim is a state-of-the-art archive of the atmospheric state calculated by the ECMWF. The data are here extracted at the grid-point nearest to Meppen Proving Ground from the $0.125^\circ \times 0.125^\circ$ spatial resolution (approximately 14×14 km). The two available times (14 and 20 h local time) nearest to the shot times (between 15 and 16 h) are considered. The corresponding profiles are shown on Fig. 7(a), together with the standard atmosphere profile. These atmospheric data are not perfectly synchronized and collocated, which is unavoidable.[38] In the future, recourse to a forecast regional model with finer temporal and spatial discretizations could partly fill this gap.[39,40]

The localization procedure of Sec. IV C has been reconducted for the 14 and 20 h ERA-Interim profiles. For the sake of comparison, the trajectories of shots 1 and 2

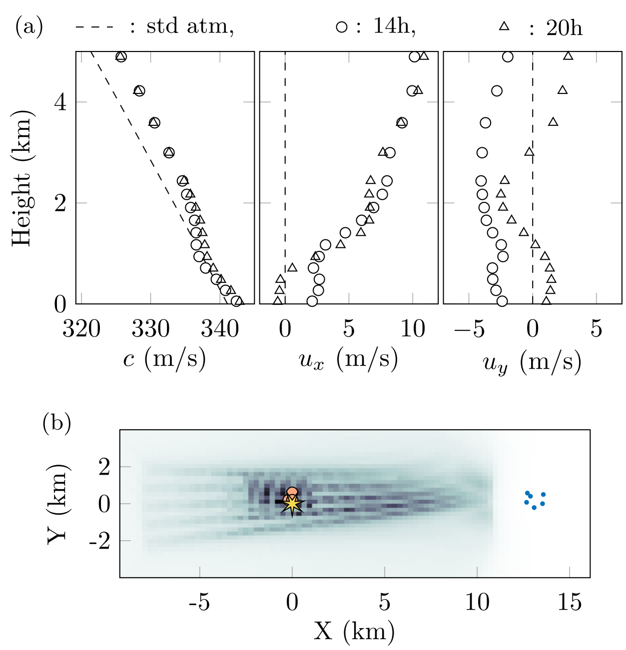

FIG. 7. (Color online) (a) Sound speed (including humidity contribution) and wind speed profiles from ERA-Interim, above Meppen, Germany, at 14 and 20 h, local time. The X and Y components of the wind (resp. u_x and u_y) are given. The vertical component is assumed to be negligible. The standard atmosphere corresponds to the dashed lines. Data points are at the database resolution. (b) Weapon's normalized localization index map for shot 3 using the 20 h profile. Same colorbar as in Fig. 4.

culminate at 1.5 km, while the trajectory of shot 3 reaches 2.5 km. For shots 1 and 2, the ranging is improved compared to the standard atmosphere case, as the estimated weapon position is within a few grid spacings (200 m) of the actual position. For shot 3, the atmospheric conditions at 14 and 20 h produce distinct localization results. The localization with the 14 h weather (not shown) is comparable to Fig. 6(f), the estimated position is off by more than 1 km. The localization obtained for 20 h is 200 m off the real position [Fig. 7(b)]. This distinct behavior may be ascribed to the wind direction change on Fig. 7(a), to which shot 3 is more sensitive because of its lower muzzle velocity and longer, higher flight. Overall, the sensitivity of weapon localizations to atmospheric conditions appears to be as expected: the localization tends to improve with the realism of the atmospheric input with no unreasonable errors.

Other physical parameters of the problem have impacts on TOAs. For example, the detachment point of the Mach wave from the projectile has a potential localization uncertainty of tens of meters, which impacts the projectile wave TOAs. TOA alterations may also result from propagation of the muzzle wave and impact wave over a non-perfectly flat ground. On the ballistics side, the data of a French 155 mm gun are used, while the actual gun is a German weapon (of the same caliber). The intrinsic variability of the internal ballistics and of the projectile's aerodynamic coefficients also lead to different trajectories and differences in the ballistic and impact waves TOAs. Exactly like the weather, all these physical effects may shift the TOAs of one wave with respect to the others. However, their TOA variation are smaller than or of the same order as the weather-induced TOA variations. The robustness noted to weather therefore supports the idea that the method is also robust to these other parameters.

B. Random TOA fluctuations

Section V A investigated the impact of weather effects, and of other parameters which can alter the TOAs of one wave relative to the others. Conversely, some physical parameters may alter the TOAs of all waves at the various microphones. For example, the TOA determination may be sensitive to the background noise in the measurements. In the considered recordings, the noise largely comes from the acquisition chain, and the signal-to-noise ratio varies between 5 (e.g., muzzle blast, shot 3) and 100 (signal saturated, most of the signatures). Artificially doubling the noise does not change the TOAs by more than a few ms. Besides, observed TOAs may be impacted by the local, instantaneous fluctuations in the atmospheric parameters (the so-called pulse wander).[10] It is argued in the Appendix that such fluctuations should not exceed standard deviation of 25 ms (25 samples) in our case.

The sensitivity to such random fluctuations is analyzed by repeating the localization procedure on all the configurations of Sec. V A (three shots, three atmospheres), but this time considering that the TOAs follow independent normal distributions around their detected value. For simplicity, a standard deviation of 25 ms is considered for all TOAs of all waves. The width of the distribution is thus of 50 samples, on the order of the maximal TOA measurement error identified in Sec. III. Actually, as the localization method works on differences of TOAs, the selected randomization test is equivalent to a test with a fixed reference TOA and all the other TOAs following a $25\sqrt{2} \sim 35$ ms standard deviation normal distribution. This general normal distribution assumption is strong and crude as all the errors may not be independent.

For each shot and atmosphere, the localization procedure in the 6-sensors configuration is carried out for 2500 realizations of the normally distributed TOAs. The position of the maximum is extracted from the index localization maps. For each shot and atmosphere, the maximal localization index may vary by a factor of 2 from realization to realization, but the position of the maximum is very consistent: the 2500 maximum positions spread over only 4–20 different (x, y) grid points depending on the shot and atmosphere, and 85% are located on just 1 to 4 grid points. This suggests a strong robustness of the peaks to TOA fluctuations. This robustness also holds when the number of microphones used to form the 2500 localization maps is decreased (see also Sec. V D). Figure 8(a) shows an example with the 3-sensors "1, 3, 5" configuration for shot 1 in the 20 h atmosphere. In spite of the small number of sensors and the large variability of the nine TOAs, the maximum falls 79% of the time on the very same database element. Two other points contain 9% of the remaining maxima. These points correspond to secondary peaks in Fig. 6(b).

In fact, it appears that the overall localization map is robust to the considered TOA fluctuations. Figure 8(b) shows the grid points whose localization index is continuously high for all the realizations. Here, the "high" criterion is defined as at least 25% of the maximum of the localization index. The patterns strongly resemble those from a single, 6-sensors realization [Fig. 6(b)]. Similar findings are obtained for other atmospheres and other shots. As may be expected, the high-index regions shrink when the threshold is raised. For a

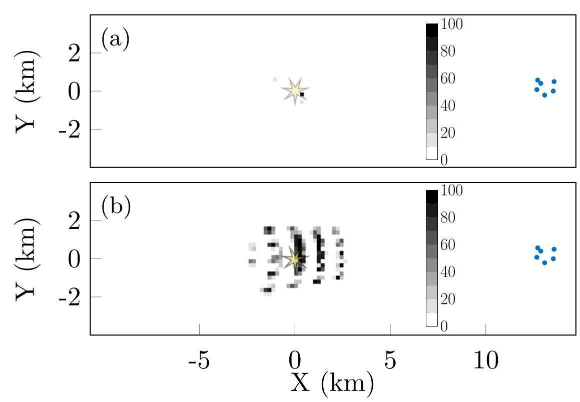

FIG. 8. (Color online) (a) Histogram of the position of the best element from the database, for shot 1, in the 20 h atmosphere, for the 3-sensors "1, 3, 5" configuration. The intensity of a grid point indicates the number of times (in %) the maximum was located on that point. (b) Stability of the localization map, for the same shot, same atmosphere and 3-sensors configuration as in (a). The intensity of a grid points indicates the number of times (in %) that the localization index at this point reaches at least 25% of the maximal localization index. The star shows the actual position of the gun.

threshold at least 75% of the maximum, the plot of Fig. 8(b) becomes similar to Fig. 8(a), for all tested configurations. The localization index map for a single realization may thus be considered as representative, even if the actual values of the localization index may fluctuate. Furthermore, the persistence of the peaks in Fig. 8(b) for random TOA fluctuations demonstrates that these peaks are not due to noise or turbulence.

C. Database discretization

The sensitivity of the localization to the discretization of the precalculated database is now investigated. Figure 9 shows the effect of refining the database for the (v, e, a) shot parameters by a factor of 5 in each dimension for shot 2 and the 20h atmosphere. The multiple peaks from the coarse database [Fig. 9(a)] disappear while the maximal localization index value rises. The other shots and atmospheric conditions considered above also lead to similar results. This shows that, at least in our tests, the cost function from Eq. (5) is physically smooth, and that the multiple peaks result from the coarse discretization of the shot parameters used to build the database.

In principle, refining the database could therefore improve the localization. However, the improvements expected from such a refinement in our cases are not spectacular. With the refined precalculation, the best matching shot varies as follows compared to the coarse precalculations: the weapon's position is shifted by 400 m along the Y direction, and its ballistic parameters (v, e, a) change by 2 m/s, 6 and 32 mils (1.75°), respectively. Thus, as illustrated on Fig. 9(b), the weapon's localizations in the coarse and refined databases are closer from each other than from the actual gun's position. This behavior is also obtained for the other shots, and in presence of random TOA fluctuations. In other words, the coarse discretization of the precalculations contributes to, but is not the major cause of, the localization errors noted above. The latter probably include some contributions from uncertainties in the meteorological conditions and of the aerodynamic coefficients.

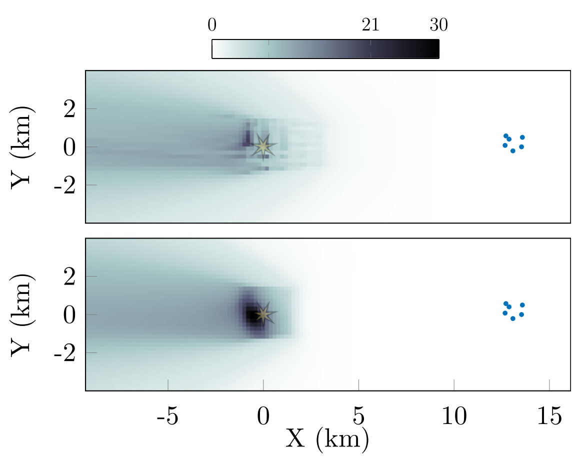

FIG. 9. (Color online) Localization index maps for shot 2 in the 20 h atmosphere, for (a) the coarsely discretized database of Secs. IV and V A–V C and (b) a refined database (2 m/s spacing for the muzzle velocity v and 2 mils for each angle e and a). The same measured TOAs are used in both cases. The maximum localization index is 21 in (a) and 30 in (b). Seventy points in (b) have a localization index above the maximum value of (a).

D. Number of sensors and array geometry

So far, the analysis has been conducted with three TOAs (from the muzzle, impact, and projectile) from the six microphones available in the experiment. Since one TOA is used for reference synchronization, this gives 17 degrees of freedom ($3 \times 6 - 1$) for a five-dimensions database (x, y, v, e, a). One may theoretically expect to achieve localization with as little as two sensors (5 degrees of freedom). To test the sensitivity to the number and geometry of sensors, the localization procedure is run for all possible combinations of k microphones, $k = 2,\ldots,6$. The case $k = 6$ corresponds to Sec. IV C. There are thus 57 combinations in total for each shot, i.e., 171 distinct sensing configurations. Here, only the results for the ERA-Interim 20 h atmospheric profile are given. The results for the 14 h atmosphere and the standard atmosphere are similar. Figure 10 shows the number of configurations corresponding to a localization less than a given value. The estimated weapon positions are consistent in most cases, for all three shots, even with two microphones. For instance, the three shot localizations obtained from microphones 4 and 5 (230 m apart, corresponding to a ratio $r \approx 0.018$), are approximately the same as those obtained with the six microphones. For $k = 3,\ldots,6$, more than 90% of the estimated positions are less than 1 km away from the actual position, and 50% are less than 300 m away. Hence, the results of Sec. IV C are robust to the geometry and the number of sensors (greater or equal to 3). The results hold when the TOAs are normally distributed around their detected value, following Sec. V B.

The limiting factor in the downsizing of the array is the uncertainty of the estimation of the TOA. The maximal measurement error was set to 50 ms in Sec. III, so about 20 m at the speed of sound. This distance qualitatively scales the minimum inter-distance between sensors in our approach.

E. Processed waves

Section IV uses the TOAs of the muzzle blast (acronym "M"), ballistic shock wave ("B"), and impact explosion ("I").

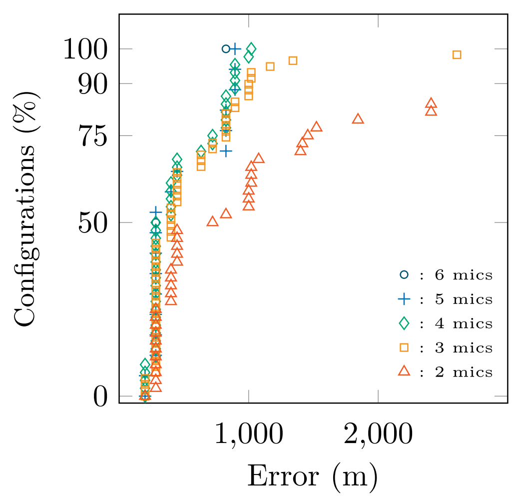

FIG. 10. (Color online) Localization results in the 20 h ERA-Interim atmosphere for a varying number of sensors. For each of the three shots, there are 1 (resp. 6, 15, 20, 15) array(s) for a subset of 6 (resp. 5, 4, 3, 2) sensors. These curves must not be interpreted as cumulative probabilities, since the data are highly correlated.

In practical scenarii, some of these data may not be available. For example, the "M" wave may be too weak to be detected due to a strongly upward refractive atmosphere (e.g., with upwind propagation in mid-afternoon summer over land). The absence of the "B" wave corresponds to a scenario with subsonic weapons like mortars. The "I" wave may be missing if there is no explosive charge (e.g., inert projectile). It is therefore of interest to assess the performance of the sensing method when one of these waves is omitted.

When the muzzle wave is not used in Eq. (5) [Fig. 11(a), using "B-I", ballistic, and impact waves], the localization performance is comparable to the "M-B-I" localization. Ignoring the "B" wave [Fig. 11(c)] leads to similar results, as the "B" and "M" waves are both informative of early steps of the trajectory, and are thus somehow redundant in constraining the weapon's position. Ignoring the "I" wave (using "M-B") produces similar results to using only the "M" wave (Sec. III). The conclusions hold when the TOAs are normally distributed around their detected value following Sec. V B.

F. Wave classification

An *a priori* assumption in Eq. (5) is that the various acoustic arrivals at the microphones have been correctly classified. In practice, this classification is not always straightforward. To assess the robustness of the approach to classification, the localization procedure is hereafter tested without prior classification of the TOAs.

With three TOAs per recording, there are $(3\times 2\times 1)^6 = 46\,656$ possible ways to combine all TOAs. However, some configurations are not physically possible for a given set of sensors positions. For example, TOAs from a single wave at different microphones must be less than 4 s apart, since all sensors are less than 1 km apart. Such simple physical considerations reduce the number of physically admissible combinations to 96, 48, and 150 for shots 1, 2, and 3, respectively. The maximum value of the localization index (C_j) further informs on the reliability of each configuration. For example, for shots 2 and 3, the maximum value of C_j is from 2 to 4 orders of magnitude larger for the correct combination of the impact and muzzle TOAs than for the other combinations. For shot 1, four distinct combinations yield similar maxima for C_j, but they all give very similar localization maps. Hence, it appears that the present approach is robust to classification, and may even be used on fully unclassified TOAs.

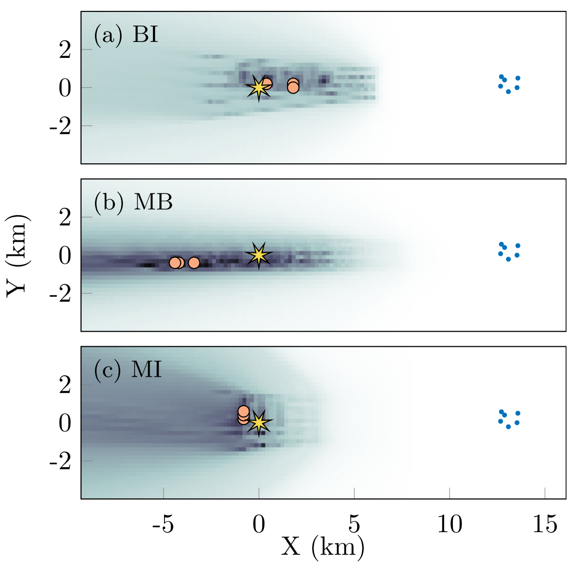

FIG. 11. (Color online) Map of the normalized localization index for various combinations of signals, for shot 2: (a) projectile and impact, (b) muzzle and projectile, (c) muzzle and impact. Same color map as in Fig. 4. The atmosphere is from ERA-Interim at 20h. Other shots lead to similar results.

VI. CONCLUSION

The acoustic sensing of artillery shots is a long-standing research challenge. One major limitation in existing techniques is the need for large baseline arrays in order to determine the weapon's position not only in bearing but also in range. In this paper, a sensing approach is introduced that demonstrates that the weapon can be located by a consistent and physical processing of all the acoustic arrivals induced by the shot.

The proposed sensing approach realistically predicts the muzzle blast, the impact explosion, and the projectile shock—the latter being obtained with the BALCO model for ballistic trajectories. The propagation of these acoustic waves in the complex environment is modeled with the IFM, which accounts for the effects of the wind, sound speed gradients, and obstacles in a reasonable computational time. Last, the time matching method combines the weapon, the projectile, and the impact acoustic data in a comprehensive localization procedure. It determines the best-matching shot parameters among a precalculated database. Besides the weapon's and impact's position, it also gives estimates for other parameters of interest, such as the shot angles, the time of flight, or the muzzle velocity of the shell.

The sensing performance of the method is tested using acoustic data from an array of six microphones for three artillery shots at the Meppen Proving Ground. The overall localization approach successfully localizes the impacts within or close to the sensors array. The weapon's location obtained by processing of the muzzle blast only, which is similar to a standard line-of-bearing processing, confirms that ranging is very poor (uncertainties of tens of kilometers). On the other hand, processing all the acoustic waves, as proposed in the present method, results in a weapon localization error of less than 1 km. Hence, the present results are very promising in that they locate the weapon with a small-baseline array. The weapon's localization uncertainties should be compared to the ballistic dispersion of 155 mm projectiles (on the order of 200 m).

An extensive sensitivity analysis of the present results is conducted. It reveals that:

- The weapon's localization is robust to realistic random TOA fluctuations.
- Use of three to five sensors instead of six produces virtually no change in the weapon's localization. Localization with two sensors is also successful in many cases.

- The localization performance does not appear to feature a major sensitivity to the orientation of the sensors with regard to the weapon.
- The method also works without prior classification of the TOAs or without processing the Mach wave (as is the case for mortar shots) or the muzzle wave.
- The noted localization errors are caused to a large extent by the imperfect knowledge on the atmospheric conditions at the time and location of the shot. Improving this knowledge (here, by recourse to weather data from a meteorological archive) directly improves the weapon's localization.
- Other localization errors may be induced by the selected discretization in the shot parameters for the precalculations and an imperfect knowledge on the aerodynamic coefficients of the projectile.

The present study conducts a careful analysis of three artillery shots. Many more configurations should be considered to quantify the method's performance in the general case. For example, it is still needed to investigate cases in which both the impact and muzzle blasts originate from positions far from the sensors. Due to the difficulty of acquiring experimental data, a fully numerical study could be considered. Localizing a virtual gun from TOAs generated by a numerical model should enable the analysis of the various relative influences of the model parameters in more detail and the optimization of the database discretization. Further studies could also be conducted to improve the database generation and search procedure in order to efficiently scan several types of weapons and several types of projectiles in several predefined types of weather. Another future development would be the recourse to meteorological data at improved spatial and temporal resolutions.

ACKNOWLEDGMENTS

We thank the BAAINBw and WTD 91 acoustic and weather data teams for their support. The ECMWF data were made available by ECMWF under the management of MeteoFrance. The contribution of D.J. was partly supported by the Labex CeLyA of Université de Lyon, operated by the French National Research Agency (ANR-10-LABX-0060/ANR-16-IDEX-0005).

APPENDIX: TURBULENCE-INDUCED TOA FLUCTUATIONS

In this Appendix, an upper bound on the turbulence-induced fluctuations of the TOAs is proposed. Cheinet *et al.*[10] discuss the turbulence-induced variations of the time-of-arrival of impulse signals (pulse wander). An estimate of the standard deviation may be found by use of their Eq. (2)

$$\Delta t = \frac{1}{c}\frac{\sigma_u}{c}\sqrt{2L_u X}, \quad \text{(A1)}$$

which proposes a quantitative evaluation of the pulse wander of impulse signals due to wind turbulence. Thermal turbulence may be considered with the above equation, but the variations are lower than for the wind-driven estimate because of the lower sensitivity of the speed of sound and comparatively smaller temperature fluctuations. In the above equation:

- σ_u is the root-mean-square (rms) of the wind speed in the direction of propagation. In the lower atmosphere, it takes values on the order of from 0.1 to 1 m/s (depending on meteorological conditions, orientation, and height; see Ref. 41, Sec. 4.3.1). Hereafter, $\sigma_u \simeq 1$ m/s is considered.
- L_u is the outer scale of wind turbulence in the direction of propagation. In the lower atmosphere, it takes values of about a hundred meters, depending on the meteorological conditions, orientation, and height. Hereafter, $L_u \simeq 200$ m is considered.
- X is the propagation range. Hereafter $X = 13$ km is considered.

With these quantitative estimates, one obtains $\Delta t \simeq 19$ ms. This corresponds to a worst-case scenario, since it considers the longest propagation range (muzzle blast), assumes strong turbulence, with large eddy scales, and fully independent turbulence paths (transverse positioning of the sensors, also ignoring the correlation in the atmospheric disturbances near the weapon). Based on these considerations, a standard deviation of $\Delta t = 25$ ms is used for all TOAs in the sensitivity study of Sec. V B. It must be stressed, though, that this value is a large overestimate as far as the impact TOA fluctuations are concerned, if only because the propagation range is much smaller.

[1] H. Bateman, "Mathematical theory of sound ranging," Monthly Weather Review (January), 4–11 (1918).
[2] E. Esclangon, *L'acoustique des Canons et des Projectiles* (Gauthier-Villars, Paris, 1925), p. 388.
[3] T. Damarla, *Battlefield Acoustics* (Springer International Publishing, New York, 2015), p. 262.
[4] A. Lemer and F. Ywanne, "Acoustic/seismic ground sensors for detection, localization and classification on the battlefield," in *Battlefield Acoustic Sensing for ISR Applications*, RTO-MP-SET-107 (US Army Research Laboratory, Adelphi, MD, 2006), pp. 17-1–17-12.
[5] B. G. Ferguson, L. G. Criswick, and K. W. Lo, "Locating far-field impulsive sound sources in air by triangulation," J. Acoust. Soc. Am. **111**(1), 104–116 (2002).
[6] A. A. Thompson III and G. L. Durfee, "Techniques for evaluating line of bearing (LOB) systems," Ballistic Research Laboratory, Aberdeen Proving Ground, MD (1992).
[7] B. G. Ferguson, "Variability in the passive ranging of acoustic sources in air using a wavefront curvature technique," J. Acoust. Soc. Am. **108**(4), 1535–1544 (2000).
[8] D. Grasing and B. Ellwood, "Development of acoustic sniper localization methods and models," Proc. SPIE **7693**, 769312 (2010).
[9] K. W. Lo, "Curvilinear trajectory estimation of a supersonic bullet using ballistic shock wave arrivals at asynchronous acoustic sensor nodes," J. Acoust. Soc. Am. **141**(6), 4543–4555 (2017).
[10] S. Cheinet, M. Cosnefroy, F. Königstein, W. Rickert, M. Christoph, S. L. Collier, A. Dagallier, L. Ehrhardt, V. E. Ostashev, A. Stefanovic, T. Wessling, and D. K. Wilson, "An experimental study of the atmospheric-driven variability of impulse sounds," J. Acoust. Soc. Am. **144**(2), 822–840 (2018).
[11] H. E. Bass, L. Sutherland, J. Piercy, and L. B. Evans, "Absorption of sound by the atmosphere," in *Physical Acoustics: Principles and Methods*, Volume 17 (A85-28596 12-71) (Academic Press, New York, 1984), pp. 145–232.
[12] S. Cheinet and T. Broglin, "Sensitivity of shot detection and localization to environmental propagation," Appl. Acoust. **93**, 97–105 (2015).

[13]S. Cheinet, L. Ehrhardt, T. Broglin, and M. Cosnefroy, "Time matching localization of impulse sounds in high-building, non-line-of-sight configurations," Acta Acust. united Ac. **102**(6), 1118–1127 (2016).
[14]S. Cheinet, L. Ehrhardt, and T. Broglin, "Impulse source localization in an urban environment: Time reversal versus time matching," J. Acoust. Soc. Am. **139**(1), 128–140 (2016).
[15]J. Millet and B. Baligand, "Latest achievements in gunfire detection systems," in *Battlefield Acoustic Sensing for ISR Applications*, RTO-MP-SET-107 (US Army Research Laboratory, Adelphi, MD, 2006), pp. 1–14.
[16]V. E. Ostashev, *Acoustics in Moving Inhomogeneous Media* (E&FN SPON, New York, 1997).
[17]A. D. Pierce, *Acoustics. An Introduction to its Physical Principles and Applications*, 3rd ed. (Acoustical Society of America, Melville, NY, 1981), pp. xxiii+642.
[18]E. W. Dijkstra, "A note on two problems in connection with graphs," Numer. Math. **1**(1), 269–271 (1959).
[19]H. Saito, "Travel times and ray paths of first arrival seismic waves: Computation method based on Huygens' principle," in *SEG Technical Program Expanded Abstracts 1989* (Society of Exploration Geophysicists, Tulsa, OK, 1989), pp. 244–247.
[20]T. J. Moser, "Shortest path calculation of seismic rays," Geophysics **56**(1), 59–67 (1991).
[21]P. Podvin and I. Lecomte, "Finite-difference computation of travel times in very contrasted velocity models: A massively parallel approach and its associated tools," Geophys. J. Int. **105**(1), 271–284 (1991).
[22]J. E. Vidale, "Finite-difference calculation of travel times," Bull. Seismol. Soc. Am. **78**(6), 2062–2076 (1988).
[23]J. A. Sethian, "A fast marching level set method for monotonically advancing fronts," Proc. Natl. Acad. Sci. **93**(4), 1591–1595 (1996).
[24]J. A. Sethian and A. B. Vladimirsky, "Ordered upwind methods for static Hamilton-Jacobi equations: Theory and algorithms," SIAM J. Numer. Anal. **41**(1), 325–363 (2003).
[25]A. M. Popovici and J. A. Sethian, "3D imaging using higher order Fast Marching travel times," Geophysics **67**(2), 604–609 (2002).
[26]J. A. Sethian and A. M. Popovici, "3D travel time computation using the Fast Marching method," Geophysics **64**(2), 516–523 (1999).
[27]Y. Pailhas and Y. Petillot, "Multi-dimensional Fast-Marching approach to wave propagation in heterogeneous multipath environment," in *Proceedings of the Third Underwater Acoustics Conference and Exhibition*, Crete, Greece (June 21–26, 2015), p. 153.
[28]E. Konukoglu, M. Sermesant, O. Clatz, J.-M. Peyrat, H. Delingette, and N. Ayache, "A recursive anisotropic Fast Marching approach to reaction diffusion equation: Application to tumor growth modeling," in *Information Processing in Medical Imaging*, edited by N. Karssemeijer and B. Lelieveldt (Springer, Berlin-Heidelberg, 2007), pp. 687–699.
[29]L. Yatziv, A. Bartesaghi, and G. Sapiro, "O(N) implementation of the fast marching algorithm," J. Comput. Phys. **212**(2), 393–399 (2006).
[30]L. Ehrhardt, S. Cheinet, D. Juvé, and P. Blanc-Benon, "Evaluating a linearized Euler equations model for strong turbulence effects on sound propagation," J. Acoust. Soc. Am. **133**(1961), 1922–1933 (2013).
[31]ISO 2533-1975, *Standard Atmosphere, Corrected* (ISO, Geneva, Switzerland, 1978).
[32]Y. Noumir, A. Le Guilcher, N. Lardjane, R. Monneau, and A. Sarrazin, "A fast-marching like algorithm for geometrical shock dynamics," J. Comput. Phys. **284**, 206–229 (2015).
[33]L. Stano, J. Wind, and H.-E. de Bree, "Acoustic scoring and locating system for rockets, artillery & mortars," in *Wireless World Workshop* (*W3*), edited by D. C. Dimitrova, K. C. H. Blom, and N. Meratnia (University of Twente, Centre for Telematics and Information Technology, Enschede, the Netherlands, 2011), pp. 1–8.
[34]P. Wey, D. Corriveau, T. A. Saitz, and W. D. Ruijter, "BALCO 6/7-DoF trajectory model," in *Proceedings of the 29th International Symposium on Ballistics*, Edenborough, Scotland (May 9–13, 2016), pp. 151–162.
[35]National Imagery and Mapping Agency, "Department of Defense World Geodetic System 1984, Its definition and relationships with local geodetic systems," Technical Report 8350.2, 3rd ed. (1984).
[36]R. F. Lieske, "Determination of aerodynamic drag and exterior ballistic trajectory simulation for the 155 mm, DPICM, M864 base-burn projectile," Ballistic Research Laboratory, Aberdeen Proving Ground, MD (1989).
[37]D. P. Dee, S. M. Uppala, A. J. Simmons, P. Berrisford, P. Poli, S. Kobayashi, U. Andrae, M. A. Balmaseda, G. Balsamo, P. Bauer, P. Bechtold, A. C. M. Beljaars, L. van de Berg, J. Bidlot, N. Bormann, C. Delsol, R. Dragani, M. Fuentes, A. J. Geer, L. Haimberger, S. B. Healy, H. Hersbach, E. V. Hólm, L. Isaksen, P. Kållberg, M. Köhler, M. Matricardi, A. P. McNally, B. M. Monge-Sanz, J.-J. Morcrette, B.-K. Park, C. Peubey, P. de Rosnay, C. Tavolato, J.-N. Thépaut, and F. Vitart, "The ERA-Interim reanalysis: Configuration and performance of the data assimilation system," Q. J. R. Meteorol. Soc. **137**(656), 553–597 (2011).
[38]D. K. Wilson, M. S. Lewis, J. W. Weatherly, and E. L. Andreas, "Dependence of predictive skill for outdoor narrowband and broadband sound levels on the atmospheric representation," Noise Control Eng. J. **56**(6), 465–477 (2008).
[39]D. Valente, L. M. Ronsse, L. Pater, M. J. White, R. Serwy, E. T. Nykaza, M. E. Swearingen, and D. G. Albert, "Blast noise characteristics as a function of distance for temperate and desert climates," J. Acoust. Soc. Am. **132**(1), 216–227 (2012).
[40]L. M. Ronsse, D. Valente, E. T. Nykaza, and M. J. White, "Investigations of measured temperature and wind effects on outdoor sound propagation," J. Acoust. Soc. Am. **132**(3), 1904–1904 (2012).
[41]R. B. Stull, *An Introduction to Boundary Layer Meteorology* (Springer, Dordrecht, the Netherlands, 1988).